

Impurity bands, line-nodes, and anomalous thermal Hall effect in Weyl superconductors

Taiki Matsushita,^{1,2} Naoyuki Kimura,³ Takeshi Mizushima,³ Ilya Vekhter,⁴ and Satoshi Fujimoto^{3,5}

¹*Department of Physics, Graduate School of Science, Kyoto University, Kyoto 606-8502, Japan*

²*Yukawa Institute for Theoretical Physics, Kyoto University, Kyoto 606-8502, Japan*

³*Department of Materials Engineering Science, Osaka University, Toyonaka, Osaka 560-8531, Japan*

⁴*Department of Physics and Astronomy, Louisiana State University, Baton Rouge, LA 70803-4001*

⁵*Center for Quantum Information and Quantum Biology, Osaka University, Toyonaka, Osaka 560-8531, Japan*

(Dated: May 17, 2024)

We investigate the anomalous thermal Hall effect (ATHE) in Weyl superconductors realized by the E_{1u} (p -wave and f -wave) chiral superconducting order for the point group D_{6h} . Using the quasiclassical Eilenberger theory, we analyze the influence of the impurity scattering and the line nodal excitations on the ATHE, and compare it with the intrinsic (topological) contribution. Because the transverse response is sensitive to the slope of the density of states at the Fermi surface, the extrinsic ATHE vanishes in both the weak (Born) and strong (unitarity) scattering limits. The thermal Hall conductivity (THC) is maximal at intermediate impurity strengths when there is a large slope of the density states in the impurity bands close to the Fermi energy. Under these conditions, the extrinsic ATHE dominates the intrinsic ATHE even at low temperatures. The extrinsic ATHE is sensitive to line nodal excitations, whereas the intrinsic ATHE is not. When the line nodes in the gap involve the sign change of the order parameter, the extrinsic contribution to the THC is suppressed even though the phase space for low energy excitation is large. In contrast, if the nodes are not accompanied by such a sign change, the extrinsic ATHE is significantly enhanced. Our results form a basis for the comprehensive analysis of anomalous thermal transport in Weyl superconductors.

I. INTRODUCTION

Weyl superconductors (WSCs) are time-reversal symmetry broken (TRSB) superconductors whose low-energy excitations behave as Weyl quasiparticles [1]. They are realized when the superconducting condensate consists of Cooper pairs with a fixed orbital angular momentum and thus are described by a complex order-parameter, $\Delta(\mathbf{k}) \propto (k_x \pm ik_y)^\nu$ ($\nu \in \mathbb{Z}$). On a three-dimensional Fermi surface centered on the Γ point, the gap closing points at $k_x = k_y = 0$ become Weyl nodes, which are sources and drains of Berry flux [2–4]. As a result, the near-nodal Bogoliubov quasiparticles behave as Weyl particles. It is common to both refer to such order parameters and label the corresponding ground states as chiral [5]. Generically, chiral superconductors with a three-dimensional Fermi surface are good candidates for the realization of WSCs.

Among the phenomena that experimentally identify WSCs are the anomalous thermal Hall effect (ATHE), a transverse thermal current driven by a temperature gradient without an applied magnetic field, and the chiral anomaly-induced phenomena, such as the torsional chiral magnetic effect and the negative thermal magnetoresistivity by textures of the order parameters [6–13]. In particular, the observation of the ATHE unambiguously identifies the chiral ground states.

At the microscopic level, there are two sources for a finite thermal Hall signal in chiral superconductors: intrinsic and extrinsic. The intrinsic mechanism is due to the geometric phase from the Berry curvature and charac-

terized by the positions of Weyl nodes in the momentum space [14–19]. The extrinsic mechanism is due to impurities and to the transfer of the angular momentum between the condensate and the quasiparticles during scattering events [20–24], which contributes both to energy-dependent skew scattering of quasiparticles on impurities and the Andreev (inter-branch, electrons to holes and vice versa) scattering. The skew scattering directly couples to the temperature gradient for $|\nu| = 1$ and results in the ATHE signal [20–22]. The Andreev mechanism only couples to impurities if the impurity potential is non- s -wave, with scattering matrix elements coupling different angular-momentum channels, and therefore appears for finite size impurities, dominating the response for $|\nu| \geq 2$ [23–25].

In this paper, we address two aspects of the ATHE in chiral superconductors with point-like impurities. First, we elucidate its origin and demonstrate the relation between the extrinsic ATHE and the evolution of the density of states (DOS) in the sub-gap impurity band, which arises from the broadening of the impurity resonant states [26, 27]. In particular, the particle-hole anisotropy, which is necessary for transverse transport, sensitively depends on the scattering phase-shift at individual impurities [28, 29]. Second, we focus on the magnitude of the thermal Hall conductivity (THC) in the situation where the winding number, ν , is not the same as the total angular momentum of the Cooper pairs, l . Such a situation often occurs when chirality coexists with additional nodes in the gap function.

Our results are relevant to several candidates of

WSCs. Historically, the Anderson-Brinkmann-Morel (ABM) state in ^3He was the first well-established Weyl superfluid with the chiral p -wave pairing [1, 30–35]. In superconducting materials, the chiral ground states over three-dimensional Fermi surfaces were proposed in a number of materials including URu_2Si_2 , UPt_3 , $\text{U}_{1-x}\text{Th}_x\text{Be}_{13}$ and SrPtAs . [15, 16, 36–55] The chiral d -wave pairing, $\Delta(\mathbf{k}) \propto k_z(k_x \pm ik_y)$, was proposed in URu_2Si_2 and explains the giant Nernst effect above the critical temperature due to preformed chiral Cooper pairs. [39, 40] Uranium compounds UPt_3 and $\text{U}_{1-x}\text{Th}_x\text{Be}_{13}$ show spin-triplet superconductivity and multiple superconducting phases as a function of tuning parameters. [56–60] While the exact order parameter symmetry in these materials is still a subject of debate, TRSB was observed in the so-called B-phase, suggesting chiral superconducting nature [43, 61]. In general, ferromagnetic superconductors show a complex “nonunitary” order parameter and support Weyl nodes on the three-dimensional Fermi surface [62–65]. Consequently, ferromagnetic UCoGe , URhGe and UGe_2 are also good candidates for the realization of WSCs [66–69].

We employ the quasiclassical method which is a hierarchical expansion in $1/(k_F\xi_0) \sim T_c/T_F \ll 1$, where k_F is the Fermi momentum, $\xi_0 = v_F/(2\pi T_c)$ is the superconducting coherence length, and T_c and T_F are the superconducting transition and the Fermi temperature respectively. Throughout the paper, we set $k_B = \hbar = 1$ for simplicity. In this language, the extrinsic contribution is of leading order, while the intrinsic mechanism is smaller by $1/(k_F\xi_0)$. Hence, understanding the extrinsic contribution is essential for correctly interpreting future experiments measuring the ATHE. However, while the intrinsic ATHE has been widely investigated in the context of topological material science [7, 16–19, 70–75], the studies of the extrinsic ATHE have been very limited. Our work thus fills this gap for Weyl superconductors.

The rest of this paper is organized as follows. We introduce the model of WSCs in Sec. II and present the expression of the THC in Sec. III. In Sec. IV, we review the quasiclassical transport (Eilenberger) theory. In Sec. IV C, the nonequilibrium Green function is calculated. The result of the low temperature analysis is given in Sec. V. In Sec. VI, we use the result of the low temperature analysis to connect the extrinsic ATHE and the formation of the impurity band. In Sec. VII, the influence of line nodal excitations on the ATHE is discussed. Section VIII is devoted to a summary and conclusion. Detailed derivation of several more complex equations in the main text is given in the Appendices.

II. MODEL

In this paper, we consider the chiral superconducting order for the point group D_{6h} and short-range impurities approximated by a delta-function potential. Table I summarizes the irreducible representations and their ba-

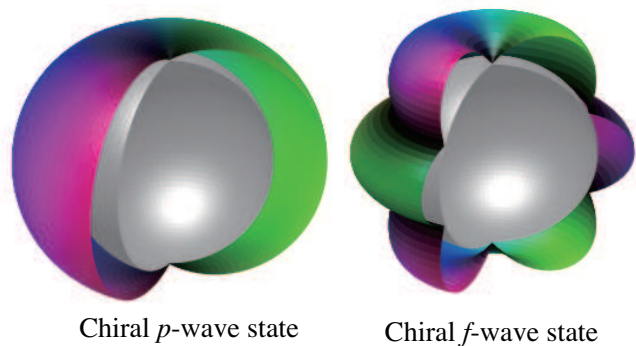


FIG. 1. The superconducting gap structures in the E_{1u} chiral superconducting states considered in the main text [see Eqs. (1) and (2)]. The left and right panels illustrate the superconducting gap structure of the chiral p -wave and E_{1u} chiral f -wave states, respectively. The color of the superconducting gap represents the phase of the complex order parameter. The grey sphere indicates the underlying Fermi sphere.

sis functions exhibiting the chiral superconducting order. [76] Among them, the skew scattering does not couple to the E_{1g} , E_{2g} and E_{2u} chiral superconducting order with the δ -function type potential. [23, 24] When impurities have finite size, the Andreev scattering couples to these chiral superconducting orders and contributes to the ATHE. Thus, the extrinsic mechanism is negligible in the E_{1g} , E_{2g} and E_{2u} chiral states when the impurity potential is short-range.

The E_{1u} chiral superconducting order has the p -wave and f -wave pairings. As shown below, these pairing states couple to the skew scattering and cause the extrinsic ATHE. Hence, we consider the p -wave and f -wave pairings in the E_{1u} state on a spherical Fermi surface.

The p -wave and f -wave chiral pairings in the E_{1u} state are expressed by,

$$\mathbf{d}(\hat{\mathbf{k}}) = \Delta(\hat{k}_x + i\hat{k}_y)\eta(\hat{k}_z)\hat{\mathbf{z}}, \quad (1)$$

with the normalized momentum $\hat{\mathbf{k}} = \mathbf{k}/k_F$. Here, $\hat{\mathbf{z}}$ represents the direction of the d -vector and k_F is the radius of the Fermi sphere. The function $\eta(\hat{k}_z)$ has to be even $\eta(\hat{k}_z) = \eta(-\hat{k}_z)$, to satisfy the requirement $\mathbf{d}(\hat{\mathbf{k}}) = -\mathbf{d}(-\hat{\mathbf{k}})$. For the chiral p -wave and f -wave pairing state, $\eta(\hat{k}_z)$ is given by,

$$\eta(k_z) = \begin{cases} 1 & \text{chiral } p\text{-wave pairing,} \\ 5\hat{k}_z^2 - 1 & \text{chiral } f\text{-wave pairing.} \end{cases} \quad (2)$$

These E_{1u} chiral order parameters generates two Weyl nodes at the north and south poles on the Fermi sphere and realizes WSCs with $\nu = 1$. As Fig. 1 shows, the E_{1u} chiral f -wave pairing involves the two horizontal line-nodes at $\hat{k}_z = \pm 1/\sqrt{5}$.

These chiral order parameters are relevant to candidate materials of WSCs. The chiral p -wave pairing, $\mathbf{d}(\hat{\mathbf{k}}) = \Delta(\hat{k}_x \pm i\hat{k}_y)\hat{\mathbf{z}}$, is established in the ABM state

of the superfluid ^3He under an ambient pressure [30–35]. Although we consider the D_{6h} symmetry, the calculated result with the chiral p -wave pairing in Eq. (2) is applicable to ^3He because we do not consider the crystalline structure except for the form of the order parameter. The E_{1u} chiral f -wave pairing is a candidate for the order parameter of UPt_3 [44, 46].

III. INTRINSIC ANOMALOUS THERMAL HALL EFFECT

In chiral superconductors, there are intrinsic and extrinsic mechanisms for the ATHE. In this section, we present the expression of the intrinsic contribution to the THC and show its low temperature behavior is completely determined by the distribution of Weyl nodes in the momentum space.

For the model presented in Sec. II, two Weyl nodes are on the k_z axis and these are separated by $\delta k_W = 2k_F$ in the momentum space. When the WSCs are regarded as a family of two-dimensional superconductors labeled by k_z , their topological nature is revealed. Each subsystem labeled by k_z is equivalent to a two-dimensional chiral superconductor and characterized by the Chern number defined as,

$$\text{Ch}(k_z) = \int \frac{dk_x dk_y}{2\pi} \sum_{E_n(\mathbf{k}) < 0} \mathcal{B}_{xy}^n(\mathbf{k}), \quad (3)$$

where $E_n(\mathbf{k})$ is the quasiparticle energy in band n , and

$$\mathcal{B}_{xy}^n(\mathbf{k}) = -2\text{Im} \left\langle \frac{\partial u_n(\mathbf{k})}{\partial k_x} \middle| \frac{\partial u_n(\mathbf{k})}{\partial k_y} \right\rangle, \quad (4)$$

is the Berry curvature. In the case of WSCs described by Eq. (1) with the positive effective mass of the normal state, the momentum-dependent Chern number becomes, [71, 72]

$$\text{Ch}(k_z) = 2\Theta(k_F^2 - k_z^2), \quad (5)$$

where $\Theta(x)$ is the Heaviside step function. The factor 2 in Eq. (5) arises from the spin degrees of freedom.

The intrinsic contribution to the thermal Hall conductivity is given by the Berry curvature formula [7, 74, 75],

$$\kappa_{xy}^{\text{int}} = -\frac{1}{2T} \sum_n \int \frac{d\mathbf{k}}{(2\pi)^3} \int_{E_n(\mathbf{k})}^{\infty} d\epsilon \epsilon^2 \mathcal{B}_{xy}^n(\mathbf{k}) \left(-\frac{\partial f}{\partial \epsilon} \right). \quad (6)$$

At low temperatures, $T \ll |\Delta|$, Eq. (6) reduces to,

$$\kappa_{xy}^{\text{int}} = \frac{\pi T}{6} \left(\frac{\delta k_W}{2\pi} \right). \quad (7)$$

Equation (7) clarifies that, at low temperatures, the intrinsic ATHE is completely determined by the distribution of Weyl nodes in the momentum space [16–19]. Note

that this low temperature formula is independent of $\eta(\hat{k}_z)$ and thus the intrinsic ATHE is insensitive to additional line nodal excitations in WSCs at least to leading order in T/T_c .

To see that the intrinsic ATHE vanishes in the standard quasiclassical limit and does not appear in the Eilenberger framework [10], let us scale the thermal conductivity by $N(\epsilon_F)v_F^2$. We find

$$\frac{\kappa_{xy}^{\text{int}}}{N(\epsilon_F)v_F^2} = \frac{\pi}{12(k_F\xi_0)} \left(\frac{T}{T_c} \right). \quad (8)$$

Equation (8) shows that the intrinsic contribution appears only at the first order in $1/(k_F\xi_0)$, whereas the standard quasiclassical theory keeps only the terms of leading (zeroth) order in $1/(k_F\xi_0)$ [see Eq. (26)]. Hence, the intrinsic contribution to the ATHE drops out in the quasiclassical Eilenberger formalism [77, 78], and we use the results above to compare with the extrinsic contribution to THC.

However, this hierarchy does not mean that the extrinsic contribution is always dominant. Recall that physically, the intrinsic ATHE is due to the gapless surface Majorana modes, which always give a T -linear contributions at low temperature, regardless of the existence of nodal excitations in bulk [6, 73, 79]. When the intrinsic contribution is derived from the bulk Hamiltonian using transport theory, the effect of the surface Majorana mode is incorporated into the THC via the correction to the Kubo formula due to the thermal magnetization current [7, 74, 75]. In contrast, whether the extrinsic ATHE exhibits T -linear behavior in the low temperature range, and, if it does, how large this contribution is, depends on the existence of nodal excitations and the location of impurity bands near the Fermi energy, see Ref. [22] and our analysis below. Therefore, whether intrinsic or extrinsic contributions dominate at low T depends on the specifics of the material.

IV. QUASICLASSICAL TRANSPORT THEORY

A. Eilenberger equation

The quasiclassical transport (Eilenberger) theory describes superconductors in the limit $1/(k_F\xi_0) \sim T_c/T_F \ll 1$. In this regime, the normal state DOS can be taken to be energy-independent over the range where the Gor'kov Green's function is peaked [77]. Integrating this Green function over the band kinetic energy, $\xi_{\mathbf{k}} = \mathbf{k}^2/2m - \epsilon_F$, we define the quasiclassical Green function as,

$$\begin{aligned} \check{g}(\epsilon, \mathbf{k}_F) &= \int d\xi_{\mathbf{k}} \check{\tau}_z \check{G}(\epsilon, \mathbf{k}) \\ &= \begin{pmatrix} \underline{g}^{\text{R}}(\epsilon, \mathbf{k}_F) & \underline{g}^{\text{K}}(\epsilon, \mathbf{k}_F) \\ 0 & \underline{g}^{\text{A}}(\epsilon, \mathbf{k}_F) \end{pmatrix}, \end{aligned} \quad (9)$$

The quasiclassical Green function is defined at the Fermi surface and is the central object of the quasiclassical

Irreducible representation	Basis function	Chirality	Parity	Extrinsic ATHE (the δ -function type impurity potential)
E_{1g}	$\hat{k}_z(\hat{k}_x \pm i\hat{k}_y)$	± 1	$+$	\times [23, 24]
E_{2g}	$(\hat{k}_x \pm i\hat{k}_y)^2$	± 2	$+$	\times [23, 24]
E_{1u}	$(\hat{k}_x \pm i\hat{k}_y)\hat{z}$	± 1	$-$	\circ [22, 24]
E_{1u}	$(5\hat{k}_z^2 - 1)(\hat{k}_x \pm i\hat{k}_y)\hat{z}$	± 1	$-$	\circ
E_{2u}	$\hat{k}_z(\hat{k}_x \pm i\hat{k}_y)^2\hat{z}$	± 2	$-$	\times [24]

TABLE I. The irreducible representations, the basis functions, the chirality, the parity, and the existence of the extrinsic ATHE due to the short-range impurity potential for the chiral superconducting order for the point group D_{6h} .

transport theory [78]. The superscript $X = R, A, K$ in Eq. (9) represents the retarded, advanced, and Keldysh matrix elements, respectively. $\tilde{\tau}_i$ ($i = x, y, z$) are the Pauli matrices in the Nambu (particle-hole) space. Throughout this paper, we denote \hat{A} as a 8×8 matrix in the Keldysh space and \underline{A} as a 4×4 Nambu matrix. If a matrix \underline{A} (\hat{A}) is defined in the Nambu (Keldysh) space, the corresponding matrix \hat{A} (\underline{A}) in the Keldysh (Nambu) space is defined as $\hat{A} = \underline{A} \otimes \mathbb{1}$.

The quasiclassical Green function obeys the Eilenberger equation [77],

$$[\epsilon\tilde{\tau}_z - \tilde{\Delta} - \check{\sigma}_{\text{imp}}, \check{g}] + i\mathbf{v}_F \cdot \nabla \check{g} = 0, \quad (10)$$

and is supplemented by the normalization condition, $\check{g}^2 = -\pi^2$. $\tilde{\Delta}$ is the superconducting order parameter matrix. For spin-triplet superconductors with the d -vector, $\mathbf{d}(\mathbf{k})$, this order parameter matrix is given by [76, 78],

$$\tilde{\Delta} = \begin{pmatrix} \underline{\Delta} & 0 \\ 0 & \underline{\Delta} \end{pmatrix}, \quad (11a)$$

$$\underline{\Delta} = \begin{pmatrix} 0 & i(\boldsymbol{\sigma} \cdot \mathbf{d}(\mathbf{k}_F))\sigma_y \\ i\sigma_y(\boldsymbol{\sigma} \cdot \mathbf{d}^*(\mathbf{k}_F)) & 0 \end{pmatrix}. \quad (11b)$$

where $\boldsymbol{\sigma} = (\sigma_x, \sigma_y, \sigma_z)$ is the vector of the Pauli matrices in the spin space. $\check{\sigma}_{\text{imp}}$ in Eq. (10) represents the impurity self-energy,

$$\check{\sigma}_{\text{imp}} = \begin{pmatrix} \underline{\sigma}_{\text{imp}}^R & \underline{\sigma}_{\text{imp}}^K \\ 0 & \underline{\sigma}_{\text{imp}}^A \end{pmatrix}. \quad (11c)$$

As mentioned before, we consider short-range charge (scalar) impurities with the δ -function type potential, $V_{\text{imp}}(\mathbf{x}) = \sum_{\mathbf{R}_{\text{imp}}} V_{\text{imp}} \delta(\mathbf{x} - \mathbf{R}_{\text{imp}})$, where \mathbf{R}_{imp} is an impurity site and V_{imp} is the potential strength. The multiple scattering events are essential for the transverse transport and thus we compute the impurity self-energy with the self-consistent T -matrix approximation. Assuming the random distribution of impurities and taking the impurity average, we obtain the self-consistent T -matrix equation [26, 27],

$$\check{\sigma}_{\text{imp}} = n_{\text{imp}} \check{t}_{\text{imp}}, \quad (12a)$$

$$\check{t}_{\text{imp}} = V_{\text{imp}} + N(\epsilon_F) V_{\text{imp}} \langle \check{g} \rangle_{\text{FS}} \check{t}_{\text{imp}}. \quad (12b)$$

where n_{imp} is the impurity density and $N(\epsilon_F)$ is the DOS at the Fermi level, ϵ_F , in the normal state. The bracket

$\langle \cdots \rangle_{\text{FS}}$ represents the normalized Fermi surface average, $\langle 1 \rangle_{\text{FS}} = 1$.

The impurity self-energy is independent of the Fermi momentum due to the short-range nature of the impurity potential. Using the scattering rate $\Gamma_{\text{imp}} = n_{\text{imp}}/\pi N(\epsilon_F)$ and the scattering phase-shift $\cot \delta = -1/\pi N(\epsilon_F) V_{\text{imp}}$ in the normal state to parameterize the impurity scattering, we recast the self-consistent T -matrix equation as

$$\check{\sigma}_{\text{imp}} = - \left[\cot \delta + \left\langle \frac{\check{g}}{\pi} \right\rangle_{\text{FS}} \right]^{-1} \Gamma_{\text{imp}} \quad (13)$$

The limit $\delta \rightarrow 0$ ($\delta \rightarrow \frac{\pi}{2}$) corresponds to the Born (unitarity) limit with the weak (strong) impurity potential.

B. Response to Temperature Gradient

The quasiclassical formalism can treat the response to the temperature gradient [80, 81]. To involve the temperature gradient in the quasiclassical theory, we consider a local equilibrium, $T = T(\mathbf{x})$, and expand the spatial gradient in Eq. (10) as $\nabla = \nabla T \frac{\partial}{\partial T}$,

$$[\epsilon\tilde{\tau}_z - \tilde{\Delta} - \check{\sigma}_{\text{imp}}, \check{g}] + (i\mathbf{v}_F \cdot \nabla T) \frac{\partial}{\partial T} \check{g} = 0. \quad (14)$$

The thermal current is given by the Keldysh component of the Green function,

$$\mathbf{J}_Q = N(\epsilon_F) \int \frac{d\epsilon}{4\pi i} \left\langle \frac{1}{4} \text{Tr} [\epsilon \mathbf{v}_F \underline{g}^K] \right\rangle_{\text{FS}}, \quad (15)$$

which we compute in the linear response theory, and then obtain the thermal conductivity tensor,

$$J_{Qi} = \kappa_{ij}^{\text{ext}} (-\partial_j T). \quad (16)$$

As shown in Sec. III, we only obtain the extrinsic contribution to the THC in this framework. [10] Hence, we add the superscript “ext” in Eq. (16) to represent the extrinsic (impurity-induced) contribution.

Once the quasiclassical limit is taken, the anomalous velocity, the effective Lorentz force in the momentum space due to Berry curvature, and side-jump effects drop out from the equations for the integrated Green function [82, 83]. As shown in Sec. III, these geometric phase

effects appear at first order in $(k_F \xi_0)^{-1}$, and accounting for them requires gradient expansion beyond the standard quasiclassical theory. [10] Consequently, when we discuss the extrinsic ATHE with the Eilenberger equation, it originates from the skew-like scattering due to chiral Cooper pairs. When we compare the extrinsic ATHE with the intrinsic one, we refer to the low temperature formula [Eq. (7)].

C. Quasiclassical Green function

With the quasiclassical transport theory, we derive the nonequilibrium Green function, which includes a linear response to the temperature gradient. Everywhere below the equilibrium functions are denoted as \tilde{x}_{eq} ($x = g, \Delta, \sigma_{\text{imp}}$) and their linear deviation from the equilibrium are labeled as $\delta\tilde{x}$ ($x = g, \Delta, \sigma_{\text{imp}}$).

1. Equilibrium Green function

In the absence of perturbations, the equilibrium Green function, \check{g}_{eq} , is obtained from Eq. (10) with the impurity self-energy given in Eq. (13). Because the Fermi surface average for the order parameter matrix vanishes, $\langle \underline{\Delta}(\mathbf{k}_F) \rangle_{\text{FS}} = 0$ due to the odd in momentum gap function, the impurity self-energy is diagonal in the Nambu space. The equation is then easily solved to obtain

$$\underline{g}_{\text{eq}}^X = -\pi \frac{M^X}{D^X} \quad \text{for } X = \text{R, A}, \quad (17)$$

$$\underline{g}_{\text{eq}}^K = \left(\underline{g}_{\text{eq}}^{\text{R}} - \underline{g}_{\text{eq}}^{\text{A}} \right) \tanh\left(\frac{\epsilon}{2T}\right), \quad (18)$$

where $M^X = \tilde{\epsilon}^X \underline{\tau}_z - \underline{\Delta}_{\text{eq}}$, $D^X = \sqrt{|\mathbf{d}(\mathbf{k}_F)|^2 - \tilde{\epsilon}^X{}^2}$ and $\tilde{\epsilon}^X = \epsilon - \frac{1}{4} \text{Tr}(\underline{\tau}_z \underline{\sigma}_{\text{imp}, \text{eq}}^X)$.

2. Nonequilibrium Green function

The nonequilibrium Green function, $\delta\check{g}$, describing the linear response to the temperature gradient obeys the Eilenberger equation,

$$\begin{aligned} & [\epsilon \tilde{\tau}_z - \check{\Delta}_{\text{eq}} - \check{\sigma}_{\text{imp}, \text{eq}}, \delta\check{g}] - [\delta\check{\Delta} + \delta\check{\sigma}_{\text{imp}}, \check{g}_{\text{eq}}] \\ & + i\mathbf{v}_F \cdot \nabla T \frac{\partial}{\partial T} \check{g}_{\text{eq}} = 0. \end{aligned} \quad (19)$$

It is straightforward to solve this equation for the retarded and the advanced Green components. Using the normalization, $\{g_{\text{eq}}^X, \delta g_{\text{eq}}^X\} = 0$ ($X = \text{R, A}$), we obtain,

$$\delta \underline{g}^X = \frac{\underline{g}_{\text{eq}}^X}{2\pi D^X} \left([\delta \underline{\sigma}_{\text{imp}}^X, \underline{g}_{\text{eq}}^X] - (i\mathbf{v}_F \cdot \nabla T) \frac{\partial}{\partial T} \underline{g}_{\text{eq}}^X \right). \quad (20)$$

The second term in Eq. (20) only depends on the temperature variations of the gap function, which is negligible at low temperatures. It can be neglected on even more

general grounds because it is traceless, and hence does not contribute to the thermal transport. Indeed, it is easy to see that $\text{Tr}(\underline{g}_{\text{eq}}^X \frac{\partial}{\partial T} \underline{g}_{\text{eq}}^X) = 2 \text{Tr} \left[\frac{\partial}{\partial T} (\underline{g}_{\text{eq}}^X)^2 \right] = 0$.

For the Keldysh component, it is convenient to define the anomalous Keldysh Green function, $\delta \underline{g}^a$, and the anomalous Keldysh impurity self-energy, $\delta \underline{\sigma}_{\text{imp}}^a$,

$$\delta \underline{g}^a = \delta \underline{g}^K - (\delta \underline{g}^{\text{R}} - \delta \underline{g}^{\text{A}}) \tanh\left(\frac{\epsilon}{2T}\right), \quad (21)$$

$$\delta \underline{\sigma}_{\text{imp}}^a = \delta \underline{\sigma}_{\text{imp}}^K - (\delta \underline{\sigma}_{\text{imp}}^{\text{R}} - \delta \underline{\sigma}_{\text{imp}}^{\text{A}}) \tanh\left(\frac{\epsilon}{2T}\right). \quad (22)$$

The second term in Eq. (21) describes the change in the spectral function, $\underline{g}^{\text{R}} - \underline{g}^{\text{A}}$ while maintaining the distribution in equilibrium. The first term in this equation accounts for the nonequilibrium distribution function and is essential for evaluating the thermal transport. This separation of the nonequilibrium Keldysh functions allows us to solve the transport equation for the Keldysh component. We obtain,

$$\delta \underline{g}^a = \delta \underline{g}_{\text{ns}}^a + \delta \underline{g}_{\text{vc}}^a, \quad (23a)$$

$$\delta \underline{g}_{\text{ns}}^a = \underline{N}_{\text{eq}}^{\text{R}} \left(\underline{g}_{\text{eq}}^{\text{R}} - \underline{g}_{\text{eq}}^{\text{A}} \right) \left(-\frac{i(\epsilon \mathbf{v}_F \cdot \nabla T)}{2T^2 \cosh^2\left(\frac{\epsilon}{2T}\right)} \right), \quad (23b)$$

$$\delta \underline{g}_{\text{vc}}^a = \underline{N}_{\text{eq}}^{\text{R}} \left(\underline{g}_{\text{eq}}^{\text{R}} \delta \underline{\sigma}_{\text{imp}}^a - \delta \underline{\sigma}_{\text{imp}}^a \underline{g}_{\text{eq}}^{\text{A}} \right), \quad (23c)$$

where we defined the retarded function

$$\underline{N}_{\text{eq}}^{\text{R}} = \frac{(D^{\text{R}} + D^{\text{A}}) \left(-\frac{\underline{g}_{\text{eq}}^{\text{R}}}{\pi} \right) + \sigma_{\text{imp}, \text{eq}0}^{\text{R}} - \sigma_{\text{imp}, \text{eq}0}^{\text{A}}}{(D^{\text{R}} + D^{\text{A}})^2 + \left(\sigma_{\text{imp}, \text{eq}0}^{\text{R}} - \sigma_{\text{imp}, \text{eq}0}^{\text{A}} \right)^2}, \quad (24)$$

with the trace of the equilibrium self-energy $\sigma_{\text{imp}, \text{eq}0}^X = \text{Tr}(\sigma_{\text{imp}, \text{eq}}^X)$ ($X = \text{R, A}$). Note that $\delta \underline{g}_{\text{vc}}^a$ involves the anomalous Keldysh impurity self-energy, which corresponds to the vertex correction in the diagrammatic calculations. We thus refer to $\delta \underline{g}_{\text{ns}}^a$ as a non-selfconsistent contribution and $\delta \underline{g}_{\text{vc}}^a$ as a vertex correction contribution, respectively.

V. THERMAL CONDUCTIVITY AT LOW TEMPERATURE

As is seen above, the anomalous Keldysh Green function is proportional to the derivative of the Fermi distribution function, $1/\cosh^2(\epsilon/2T)$. This factor introduces the frequency cut-off $\epsilon \sim T$, which becomes small at low temperatures, justifying the expansion of the Green function in ϵ [22]. We utilize this low temperature expansion to determine the low temperature behavior of the extrinsic ATHE in WSCs.

Following the procedure outlined in Ref. [22], we obtain the low temperature expansion for the thermal conduc-

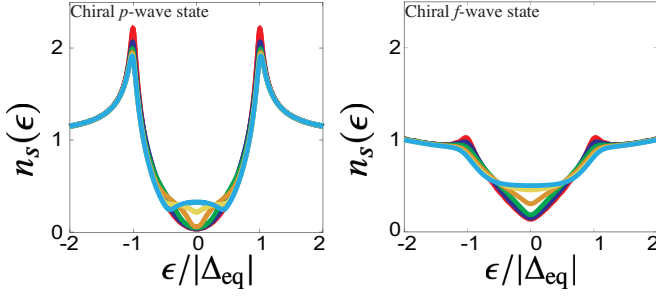


FIG. 2. The quasiparticle DOS for the WSCs with the E_{1u} chiral pairings for the several values of the scattering phase-shift. In this calculation, we set the scattering rate as $\Gamma_{\text{imp}} = 0.04\pi T_{c,\text{clean}}$ ($T_{c,\text{clean}}$ is a critical temperature in clean systems) and the scattering phase-shift as $\delta = \frac{\pi}{12}$ (red lines), $\frac{\pi}{6}$ (blue lines), $\frac{\pi}{4}$ (green lines), $\frac{\pi}{3}$ (orange lines), $\frac{5\pi}{12}$ (yellow lines), $\frac{\pi}{2}$ (sky blue).

tivity in WSCs as [84],

$$\begin{aligned} \frac{\kappa_{yy}^{\text{ext}}}{N(\epsilon_F)v_F^2} &\simeq \frac{\pi^2 T}{6} \gamma^2 \langle \alpha_0(\hat{k}_z) \rangle_{\text{FS}} \\ &\quad + \frac{\pi^2 \Gamma_{\text{imp}} \gamma^2 |\Delta_{\text{eq}}|^2 T}{3} Y \langle \alpha_1(\hat{k}_z) \rangle_{\text{FS}}^2 \\ &\quad + \mathcal{O}(T^2, \Gamma_{\text{imp}}^4), \end{aligned} \quad (25)$$

$$\begin{aligned} \frac{\kappa_{xy}^{\text{ext}}}{N(\epsilon_F)v_F^2} &\simeq - \frac{\pi^2 \Gamma_{\text{imp}} \gamma^2 |\Delta_{\text{eq}}|^2 T}{3} X \langle \alpha_1(\hat{k}_z) \rangle_{\text{FS}} \\ &\quad + \mathcal{O}(T^2, \Gamma_{\text{imp}}^4), \end{aligned} \quad (26)$$

with $i\gamma \equiv -\frac{1}{4}\text{Tr}[\mathcal{I}_z \sigma_{\text{imp,eq}}^R(\epsilon=0)]$. In Appendix B, we derive the complete expression for the thermal conductivity at the low temperature, including higher-order terms in the scattering rate, Γ_{imp} . Note that the extrinsic contribution has the opposite sign of the intrinsic contribution when the impurity potential is attractive for electrons ($0 < \delta < \pi/2$) [22]. In Eqs. (25)-(26), the dimen-

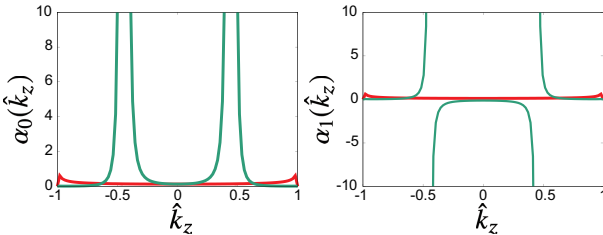


FIG. 3. \hat{k}_z -dependence of the functions α_0 and α_1 in the WSCs with the E_{1u} chiral pairings [see Eqs. (25)-(26)]. The red and green curves show the chiral p -wave and f -wave chiral pairings, respectively. We set the scattering rate $\Gamma_{\text{imp}} = 0.04\pi T_{c,\text{clean}}$ and the phase-shift $\delta = \frac{\pi}{6}$.

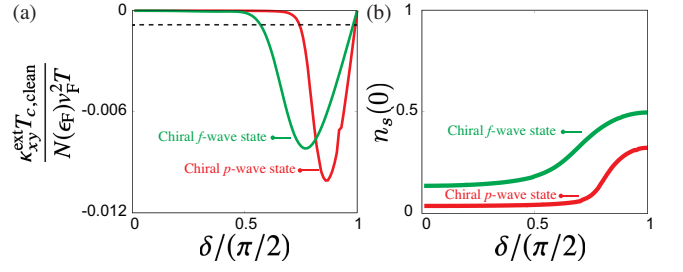


FIG. 4. Effect of the scattering phase shift. (a) The scattering phase-shift dependence of the extrinsic ATHE in WSCs at the low temperature. (b) The phase-shift dependence of the zero-energy DOS. In the panel (a), the dotted line plots $-\kappa_{xy}^{\text{int}}$ with $1/(k_F \xi_0) = 0.01$, where the minus sign of $-\kappa_{xy}^{\text{int}}$ is due to compare the relative magnitude with κ_{xy}^{ext} . In these calculations, we set the scattering rate as $\Gamma_{\text{imp}} = 0.04\pi T_{c,\text{clean}}$ and the temperature as $T = 0.02T_{c,\text{clean}}$.

sionless factors X and Y are defined as,

$$X = \frac{n_s(0) \cot \delta}{2(\cot^2 \delta + n_s^2(0))^2}, \quad (27a)$$

$$Y = \frac{\cot^2 \delta - n_s^2(0)}{4(\cot^2 \delta + n_s^2(0))^2}, \quad (27b)$$

with $n_s(\epsilon) = \frac{N_s(\epsilon)}{N(\epsilon_F)}$. $N_s(\epsilon)$ is the quasiparticle DOS,

$$N_s(\epsilon) = N(\epsilon_F) \left\langle -\frac{1}{4} \text{Tr} \text{Im} \left(\frac{g_{\text{eq}}^R(\epsilon)}{\pi} \right) \right\rangle_{\text{FS}}. \quad (28)$$

In Fig. 2, we plot the quasiparticle DOS in the E_{1u} chiral p -wave and f -wave states. The Fermi surface function $\alpha_n(\hat{k}_z)$ ($n \in \mathbb{Z}$), is defined as

$$\alpha_n(\hat{k}_z) = \frac{\hat{k}_\perp^2 \eta^n(\hat{k}_z)}{(\gamma^2 + |\Delta_{\text{eq}} \hat{k}_\perp \eta(\hat{k}_z)|^2)^{\frac{3}{2}}}, \quad (29)$$

with $\hat{k}_\perp^2 = \hat{k}_x^2 + \hat{k}_y^2 = 1 - \hat{k}_z^2$. $\eta(\hat{k}_z)$ is defined in Sec. II and describes the additional nodal and near-nodal structures.

As shown in Fig. 3 (a), $\alpha_0(\hat{k}_z)$ is sharply peaked at the positions of the line-nodes on the Fermi surface, because the denominator in Eq. (29) is small in these regions. Hence, as may be expected, low-energy quasiparticles near nodal lines enhance the longitudinal thermal transport. On the other hand, $\alpha_1(\hat{k}_z)$ in Fig. 3(b) changes its sign across the line node due to $\eta(\hat{k}_z)$ in the numerator of Eq. (29) (see also Fig. 1). As we show below, this sign change at line-nodes significantly affects the extrinsic ATHE.

The factors X and Y stem from the vertex correction of the nonequilibrium Keldysh Green function and describe the nature of impurity bound states in superconductors [28, 29]. Because only unpaired quasiparticles

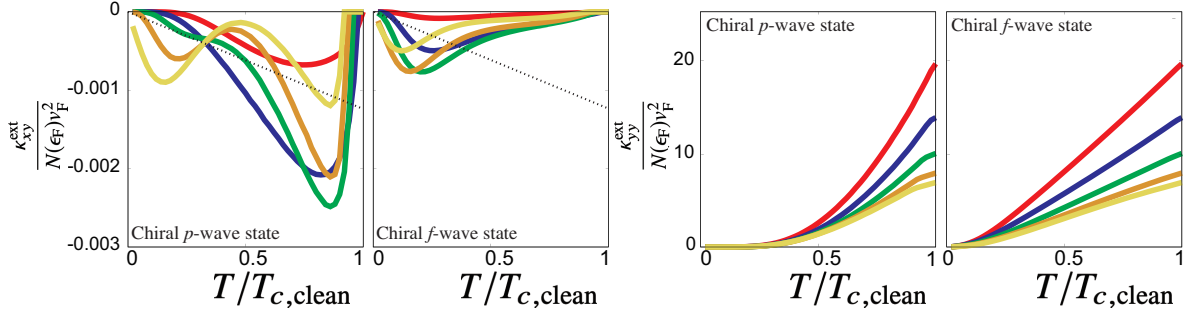


FIG. 5. Temperature dependence of the extrinsic ATHE in the WSCs with the E_{1u} chiral pairings. In all panels, we set the scattering rate as $\Gamma = 0.04\pi T_c$ and the scattering phase-shift as $\delta = \frac{\pi}{12}$ (red lines), $\frac{\pi}{6}$ (blue lines), $\frac{\pi}{4}$ (Green lines), $\frac{\pi}{3}$ (orange lines), $\frac{5\pi}{12}$ (yellow lines). The dotted lines plot $-\kappa_{xy}^{\text{int}}$ using the low temperature formula with $1/(k_F \xi_0) = 0.01$, where the minus sign of $-\kappa_{xy}^{\text{int}}$ is due to compare the relative magnitude with κ_{xy}^{ext} .

carry entropy, a finite residual (zero-energy) DOS is a necessary, but not sufficient, condition to obtain a finite THC [see Eq. (26)]. As shown in Fig. 4(a), the THC vanishes both in the Born ($\delta \rightarrow 0$) and unitarity ($\delta \rightarrow \frac{\pi}{2}$) limit, and exhibits a peak at intermediate the scattering phase-shift. The key observation is that the thermal Hall signal is enhanced by the effective DOS anisotropy at the Fermi surface, i.e., the finite slope of the DOS as a function of energy near $\epsilon = 0$. This slope vanishes in both unitarity and Born limit as shown in Fig. 2, but $(\partial N_s / \partial \epsilon)_{\epsilon=0} \neq 0$ is realized in the intermediate range of the scattering phase-shift. As discussed in Sec. III, the quasichlassical method does not capture the intrinsic contribution to the THC, and hence, the THC from Eq. (26) vanishes in both limits. In Sec. VI, we clarify the relation between the extrinsic ATHE and the emergence of the impurity band.

Importantly, even at low temperatures, the extrinsic contribution is comparable to the intrinsic contribution when $\delta \gtrsim 0.75\pi$ ($\delta \gtrsim 0.55\pi$) in the chiral $p(f)$ -wave state [see Fig. 4(a)].

VI. IMPURITY BOUND STATES AND ANOMALOUS THERMAL HALL EFFECT

We now demonstrate explicitly how the extrinsic ATHE is closely related to the emergence of the impurity bound states in superconductors. Recall that in unconventional superconductors with a momentum-dependent gap function, multiple Andreev scattering at impurities creates the quasiparticle bound states. This impurity band affects the quasiparticle DOS, especially near the unitarity limit, as seen Fig. 2 [26, 27]. As the phase-shift of impurity scattering deviates from the unitarity, the energy of the individual bound states moves to a finite energy. For weak scatterers, the spectral weight for the bound states is eventually absorbed in the coherence peaks around $\epsilon \simeq \pm |\Delta_{\text{eq}}|$.

From the T -matrix equation in equilibrium and the zero-energy DOS, we find the relationship between the

extrinsic ATHE and the DOS,

$$\frac{\kappa_{xy}^{\text{ext}}}{N(\epsilon_F) v_F^2} = -\frac{\pi^2 \Gamma_{\text{imp}} \gamma^2 T}{12} \frac{\langle \alpha_1(\hat{k}_z) \rangle_{\text{FS}}^2}{\langle \alpha_2(\hat{k}_z) \rangle_{\text{FS}}} \frac{\partial n_s(0)}{\partial \delta} \sin^2 \delta + \mathcal{O}(T^2, \Gamma_{\text{imp}}^4). \quad (30)$$

Equation (30) is derived in Appendix C. Equation (30) shows that the ATHE is closely related to the scattering phase-shift dependence of the residual DOS, $\frac{\partial n_s(0)}{\partial \delta}$, which is characterized by the emergence of the impurity bound states. As seen in Fig. 4(b), the zero-energy DOS rapidly grows in the intermediate scattering phase-shift. The variation of $n_s(0)$ with δ slows down and eventually saturates in the unitarity limit. This evolution of the zero-energy DOS qualitatively agrees with the phase-shift dependence of the ATHE in WSCs.

VII. LINE-NODES AND ANOMALOUS THERMAL HALL EFFECT

A. Chiral p -wave state v.s. chiral f -wave state

We are now in the position to compare the full numerical evaluation results for the thermal transport for the E_{1u} chiral p -wave and f -wave states, showing the influence of additional line-nodes on the extrinsic ATHE. As predicted by the low temperature expansion analysis, the extrinsic ATHE is small both for weak (Born) and strong (unitarity) scatterers and reaches the largest value for the intermediate phase-shift (see Fig. 5).

The relative magnitude between the intrinsic and extrinsic ATHE is consistent with the result of the low temperature expansion analysis [see Figs. 4(a) and 5]. Assuming that the intrinsic contribution to the THC exhibits T -linear and unaltered at higher temperatures, the intrinsic mechanism should dominate over the extrinsic contribution at higher temperatures. However, in that range, we generally expect corrections to the result in Eq. (7).

Notably, the maximum amplitude of the THC in the chiral f -wave state with two horizontal line-nodes is smaller than that of the chiral p -wave state. This is in sharp contrast with the longitudinal thermal transport which is enhanced by the enlarged phase spaces available to quasiparticles near nodal lines. This result implies that the extrinsic ATHE is weakened by additional line nodes. This observation is consistent with the low temperature analysis discussed in Sec. V. The function $\alpha_1(\hat{k}_z)$ is proportional to $\eta(\hat{k}_z)$ [see Eqs. (1) and (29)] and changes sign across the additional line-nodes, as illustrated in Fig. 3. It is precisely that this sign change reduces the Fermi surface average of this function and suppresses the extrinsic anomalous thermal Hall response.

B. Coexistence of the chiral p -wave and f -wave pairings

Both the chiral p -wave and f -wave pairings we considered belong to the E_{1u} irreducible representation and hence these are naturally mixed. [76] We denote the chiral p (f)-wave order parameter as $\Delta_{p(f)}$ and write the order parameter in the mixed pairing state as,

$$\mathbf{d}(\mathbf{k}_F) = \Delta_f(\hat{k}_x + i\hat{k}_y) \left(5\hat{k}_z^2 - 1 + \frac{\Delta_p}{\Delta_f} \right) \hat{z}. \quad (31)$$

This order parameter in the mixed pairing state is written as Eq. (1) with $\eta(\hat{k}_z) = 5\hat{k}_z^2 - 1 + \Delta_p/\Delta_f$.

The nodal structure of the resulting gap depends on the ratio Δ_p/Δ_f . There are always Weyl nodes at the north and south poles of a spherical Fermi surface. In addition, the superconducting gap has two line-nodes when $-4 < \Delta_p/\Delta_f < 1$. These nodes merge at the equator for $\Delta_p/\Delta_{E_{1u}} = 1$, and, for $\Delta_p/\Delta_f > 1$, the equatorial line-node is lifted, and replaced by a minimum (see Fig. 6 (b)).

As seen in Fig. 6 (b), the extrinsic ATHE is enhanced when the two horizontal line-nodes merge at the equator. When the mixed chiral state possesses a single line-node or small line-node gap minima at the equator, the extrinsic ATHE becomes dominant at low temperatures. When the line-node at the equator splits into two, the extrinsic ATHE is sharply suppressed. As shown in Fig. 6 (c), the small gap minima also suppresses the extrinsic ATHE, but the suppression by the gap minima is more gradual.

This behavior is also understood from the low temperature formula for the extrinsic ATHE (Eq. 26)). As shown in Fig. 7, when we introduce the chiral p -wave gap to the chiral f -wave state with $0 < \Delta_p/\Delta_{E_{1u}} < 1$, two line-nodes get closer to each other. When two line-nodes approach each other, the positive region of $\alpha_1(\hat{k}_z)$ is enlarged, and its momentum average is enhanced. As shown in Fig. 7, when two line-nodes merge at the equator, there is no sign change of the gap function and $\alpha_1(\hat{k}_z)$ becomes a positive function. Absence of the sign change at line-nodes enhances the extrinsic ATHE since

now the contribution of additional quasiparticles in the near-nodal regions (appearing in the denominator of α_1 in Eq. (29)) is not reduced by the sign change in the numerator on performing the Fermi surface average.

VIII. CONCLUSION

In this paper, we addressed the relative magnitude of the intrinsic and extrinsic ATHE in WSCs. The intrinsic ATHE arises from the existence of Weyl nodes and boundary modes and is determined by the structure of the order parameter and the distribution of Weyl nodes in the momentum space. The extrinsic contribution is due to the skew scattering of quasiparticles. We computed the extrinsic contribution to the THC using the quasi-classical Eilenberger formalism. The intrinsic ATHE is suppressed by the small factor, $1/(k_F\xi_0)$, in superconductors, and thus the extrinsic contribution often dominates the thermal Hall responses. The intrinsic contribution relies on the gapless boundary modes and exhibits T -linear behavior regardless of the existence of nodal excitation in bulk [79]. Thus, the intrinsic contribution may dominate the thermal Hall response at low temperatures when the impurity potential is weak. Within this formalism, we combined the low temperature analysis and the numerical calculations to specifically focus on the effects of the impurity bands and the additional nodal structure on the extrinsic ATHE.

One of our findings is that the variation of the density of states near the Fermi energy is crucial in determining the transverse transport coefficients. We find that impurities with the intermediate potential strength are more effective in generating the thermal Hall signal than those in the weak (Born) or strong (unitarity) scattering limit. We confirmed this by investigating the phase-shift dependence of the DOS and the ATHE, and associated the result with the growth of the impurity band from the individual impurity resonances.

We showed that the additional line nodal structure significantly reduces the extrinsic contribution to the THC when line-nodes involve the sign change of the order parameter. For such order parameters, the angular momentum of the Cooper pairs is not the same as the winding number around the nodes. Consequently, the skew scattering from different parts of the Fermi surface partially compensates. In contrast, when the line nodes are not accompanied by such a sign change, quasiparticle excitations around the gap minima significantly enhance the thermal Hall response.

Our results can be applied to any chiral superconductor even without Weyl nodes. For an example, we note the chiral d -wave pairing, $\Delta(\mathbf{k}) \propto \hat{k}_z(\hat{k}_x \pm i\hat{k}_y)$ among candidate order parameters for Sr_2RuO_4 [85]. The chiral d -wave order parameter does not realize Weyl nodes because this compound has quasi-two-dimensional Fermi surfaces and the Fermi surface is absent at $k_x = k_y = 0$. However, the chiral d -wave superconducting order in-

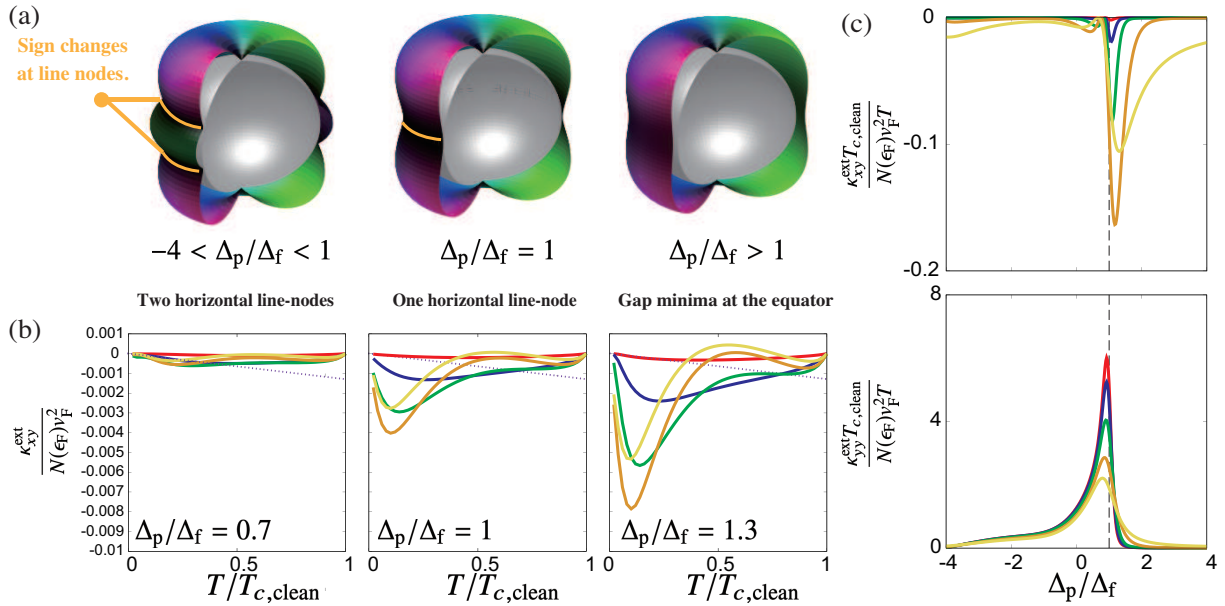


FIG. 6. Anomalous Thermal Hall Effect in Weyl superconductors. (a) Temperature dependence of the extrinsic ATHE in the mixed state of the chiral p -wave state and the E_{1u} chiral f -wave state. (b) $\Delta_p/\Delta_{E_{1u}}$ dependence of the thermal conductivity at low temperature, $T = 0.02T_{c, \text{clean}}$. We set the scattering phase-shift $\delta = \frac{\pi}{12}$ (red lines), $\frac{\pi}{6}$ (blue lines), $\frac{\pi}{4}$ (Green lines), $\frac{\pi}{3}$ (orange lines), $\frac{5\pi}{12}$ (yellow lines). (c) Schematic picture of the gap structures of the mixed chiral state model. The dotted lines in the panel (a) plot $-\kappa_{xy}^{\text{int}}$ using the low temperature formula, where the minus sign of $-\kappa_{xy}^{\text{int}}$ is due to compare the relative magnitude with κ_{xy}^{ext} . The dashed lines in the panel (b) describe Δ_p/Δ_f where two line-nodes merge into one.

volves the broken time-reversal and mirror reflection symmetries, allowing the ATHE [22]. Because the chiral d -wave order parameter realizes a line node at $k_z = 0$ with the sign change, the line nodal excitations suppress the extrinsic ATHE. Hence, the intrinsic contribution will be a substantial part of ATHE in Sr_2RuO_4 , but the detailed balance between it and the extrinsic contribution depends on the details of the Fermi surface and other material-specific parameters.

Our findings provide clear evidence that in large classes of candidate materials, there is likely to be a competition between the intrinsic and extrinsic contributions to the ATHE even at the low temperature, and careful (and potentially material-specific) analysis is needed to understand its behavior in the superconducting state. Our

work lays the framework and provides the blueprint for such analysis.

ACKNOWLEDGMENTS

T. Matsuhita thank Y. Masaki, M. Sato, Y. Yanase, Y. Tanaka, and J. Ieda for fruitful discussions. T. Matsuhita was supported by a Japan Society for the Promotion of Science (JSPS) Fellowship for Young Scientists and by JSPS KAKENHI Grant No. JP19J20144 and JST CREST Grant No. JPMJCR19T2. This work was also supported by JST CREST Grant No. JPMJCR19T5, Japan, and JSPS KAKENHI (Grants No. JP21H01039 and No. JP22H01221). I. V. was supported in part by grant NSF PHY-1748958 to the Kavli Institute for Theoretical Physics (KITP).

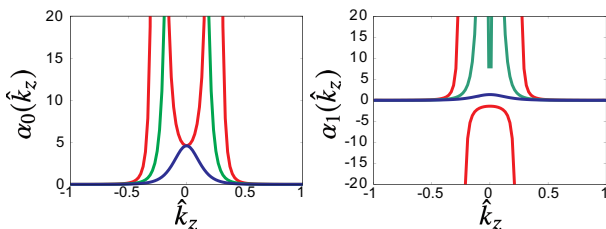


FIG. 7. \hat{k}_z -dependence of the functions α_0 and α_1 for the mixed chiral state model. The red, blue and green curves show the calculated results with $\Delta_p/\Delta_{E_{1u}} = 0.7, 1, 1.3$, respectively. We set the scattering rate as $\Gamma_{\text{imp}} = 0.04\pi T_{c, \text{clean}}$ and the phase-shift as $\delta = \frac{\pi}{6}$.

Appendix A: Derivation of Eqs. (23a), (23b), and (23c)

In this appendix, we derive the linear response of anomalous Keldysh Green function, $\delta\tilde{g}^a$, to a temperature gradient. We start from the Eilenberger equation

for the non-equilibrium Keldysh Green function, $\delta\tilde{g}^K$,

$$\begin{aligned} & (\underline{M}^R \delta\tilde{g}^K - \delta\tilde{g}^K \underline{M}^A) - (\sigma_{\text{imp,eq0}}^R - \sigma_{\text{imp,eq0}}^A) \delta\tilde{g}^K \\ & + (\underline{\sigma}_{\text{imp,eq}}^K \delta\tilde{g}^A - \delta\tilde{g}^R \underline{\sigma}_{\text{imp,eq}}^K) - \left(\delta\underline{\sigma}_{\text{imp}}^R \underline{g}_{\text{eq}}^K - \underline{g}_{\text{eq}}^K \delta\underline{\sigma}_{\text{imp}}^A \right) \\ & - \left(\delta\underline{\sigma}_{\text{imp}}^K \underline{g}_{\text{eq}}^A - \underline{g}_{\text{eq}}^R \delta\underline{\sigma}_{\text{imp}}^K \right) + (i\mathbf{v}_F \cdot \nabla T) \frac{\partial}{\partial T} \underline{g}_{\text{eq}}^K = 0. \end{aligned} \quad (\text{A1})$$

With the anomalous Keldysh Green function, $\delta\tilde{g}^a$, and the anomalous Keldysh impurity self-energy, $\delta\underline{\sigma}_{\text{imp}}^a$, we recast Eq. (A1) into,

$$\begin{aligned} & (\underline{M}^R \delta\tilde{g}^a - \delta\tilde{g}^a \underline{M}^A) - (\sigma_{\text{imp,eq0}}^R - \sigma_{\text{imp,eq0}}^A) \delta\tilde{g}^a \\ & + \left(\underline{g}_{\text{eq}}^R \delta\underline{\sigma}^a - \delta\underline{\sigma}^a \underline{g}_{\text{eq}}^A \right) - \frac{i(\epsilon\mathbf{v}_F \cdot \nabla T)}{2T^2 \cosh^2\left(\frac{\epsilon}{2T}\right)} \left(\underline{g}_{\text{eq}}^R - \underline{g}_{\text{eq}}^A \right) = 0. \end{aligned} \quad (\text{A2})$$

The anomalous Keldysh impurity self-energy is calculated from the T -matrix equation,

$$\begin{aligned} \delta\underline{\sigma}_{\text{imp}}^a &= \Gamma_{\text{imp}} \left(\cot \delta + \left\langle \frac{\underline{g}_{\text{eq}}^R}{\pi} \right\rangle_{\text{FS}} \right)^{-1} \\ & \times \left\langle \frac{\delta\underline{g}^a}{\pi} \right\rangle_{\text{FS}} \left(\cot \delta + \left\langle \frac{\underline{g}_{\text{eq}}^A}{\pi} \right\rangle_{\text{FS}} \right)^{-1}. \end{aligned} \quad (\text{A3})$$

The anomalous Keldysh Green function satisfies $\underline{g}_{\text{eq}}^R \delta\tilde{g}^a + \delta\tilde{g}^a \underline{g}_{\text{eq}}^A = 0$. Using this normalization, we can solve the transport equation, (A2), and obtain the anomalous Keldysh Green function,

$$\delta\tilde{g}^a = \delta\underline{g}_{\text{ns}}^a + \delta\underline{g}_{\text{vc}}^a, \quad (\text{A4})$$

$$\delta\underline{g}_{\text{ns}}^a = \underline{N}_{\text{eq}}^R \left(\underline{g}_{\text{eq}}^R - \underline{g}_{\text{eq}}^A \right) \left(-\frac{i(\epsilon\mathbf{v}_F \cdot \nabla T)}{2T^2 \cosh^2\left(\frac{\epsilon}{2T}\right)} \right), \quad (\text{A5})$$

$$\delta\underline{g}_{\text{vc}}^a = \underline{N}_{\text{eq}}^R \left(\underline{g}_{\text{eq}}^R \delta\underline{\sigma}_{\text{imp}}^a - \delta\underline{\sigma}_{\text{imp}}^a \underline{g}_{\text{eq}}^A \right), \quad (\text{A6})$$

where

$$\underline{N}_{\text{eq}}^R = \frac{(D^R + D^A) \left(-\frac{\underline{g}_{\text{eq}}^R}{\pi} \right) + \sigma_{\text{imp,eq0}}^R - \sigma_{\text{imp,eq0}}^A}{(D^R + D^A)^2 + \left(\sigma_{\text{imp,eq0}}^R - \sigma_{\text{imp,eq0}}^A \right)^2}. \quad (\text{A7})$$

Appendix B: Derivation of Eqs. (25) and (26)

At low temperature, we expand the Green function in the energy ϵ , because we expect the energy range to be cut off by the temperature, while the Green function varies on the scale of the superconducting gap. As seen in the main text, the non-equilibrium retarded and advanced functions do not contribute to thermal transport because they arise from the temperature dependence

of the equilibrium gap function. We thus focus on the anomalous Keldysh Green function. To the leading order in ϵ , the anomalous Keldysh Green function, Eqs. (23a)-(23c) reduce to,

$$\delta\underline{g}_{\text{LT}}^a = \delta\underline{g}_{\text{ns,LT}}^a + \delta\underline{g}_{\text{vc,LT}}^a, \quad (\text{B1})$$

$$\begin{aligned} \delta\underline{g}_{\text{ns,LT}}^a &= -\frac{\underline{g}_{\text{eq,LT}}^R}{2\pi D_{\text{LT}}} \left(\underline{g}_{\text{eq,LT}}^R - \underline{g}_{\text{eq,LT}}^A \right) \\ & \times \left(-\frac{i(\epsilon\mathbf{v}_F \cdot \nabla T)}{2T^2 \cosh^2\left(\frac{\epsilon}{2T}\right)} \right), \end{aligned} \quad (\text{B2})$$

$$\begin{aligned} \delta\underline{g}_{\text{vc,LT}}^a &= -\frac{\underline{g}_{\text{eq,LT}}^R}{2\pi D_{\text{LT}}} \\ & \times \left(\underline{g}_{\text{eq,LT}}^R \delta\underline{\sigma}_{\text{imp,LT}}^a - \delta\underline{\sigma}_{\text{imp,LT}}^a \underline{g}_{\text{eq,LT}}^A \right). \end{aligned} \quad (\text{B3})$$

Here the subscript ‘‘LT’’ denotes the zero-frequency limit, $\epsilon = 0$. In that limit, the impurity self-energy $\sigma_{\text{imp,eq0}}$ in equilibrium is purely real and the retarded and advanced values are identical. $\underline{g}_{\text{eq,LT}}^{\text{R(A)}}$ is given by,

$$\underline{g}_{\text{eq,LT}}^R = -\pi \frac{i\gamma \mathcal{I}_z - \Delta_{\text{eq}}}{D_{\text{LT}}}, \quad (\text{B4})$$

$$\underline{g}_{\text{eq,LT}}^A = -\pi \frac{-i\gamma \mathcal{I}_z - \Delta_{\text{eq}}}{D_{\text{LT}}}, \quad (\text{B5})$$

with $D_{\text{LT}} \equiv D_{\text{LT}}^R = D_{\text{LT}}^A = \sqrt{\gamma^2 + |\Delta_{\text{eq}} \hat{k}_{F\perp} \eta(\hat{k}_z)|^2}$. The self-energy $\sigma_{\text{imp,LT}}^R = -i\gamma \mathcal{I}_z$ in equilibrium is calculated from the T -matrix equation,

$$\gamma = \Gamma_{\text{imp}} \frac{n_s(0)}{\cot^2 \delta + n_s^2(0)}, \quad (\text{B6})$$

with the zero-energy DOS,

$$n_s(0) = \left\langle \frac{\gamma}{\sqrt{|\Delta_{\text{eq}} \hat{k}_{F\perp} \eta(\hat{k}_z)|^2 + \gamma^2}} \right\rangle_{\text{FS}}. \quad (\text{B7})$$

Here, we assume a spatially uniform temperature gradient along the y -direction and $\Delta_{\text{eq}} \in \mathbb{R}$. As in the manuscript, we consider the d -vector fixed along the z axis. In this case, the spin along the z axis is conserved, which allows us to focus on each spin subspace. Hence, we perform the low temperature expansion in each spin subspace and drop the spin index. In the zero-frequency limit, the anomalous Keldysh impurity self-energy is calculated from the self-consistent T -matrix equation,

$$\begin{aligned} \delta\underline{\sigma}_{\text{imp,LT}}^a &= \frac{\Gamma_{\text{imp}}}{(\cot^2 \delta + n_s^2(0))^2} (\cot \delta + in_s(0) \mathcal{I}_z) \\ & \times \left\langle \frac{\delta\underline{g}_{\text{ns,LT}}^a + \delta\underline{g}_{\text{vc,LT}}^a}{\pi} \right\rangle_{\text{FS}} (\cot \delta - in_s(0) \mathcal{I}_z). \end{aligned} \quad (\text{B8})$$

The Fermi surface average of the non-selfconsistent contribution, $\delta\underline{g}_{\text{ns,LT}}^a$ can be straightforwardly performed.

From Eq. (B2), we obtain,

$$\begin{aligned} & \frac{\Gamma_{\text{imp}}}{(\cot^2 \delta + n_s^2(0))^2} (\cot \delta + in_s(0) \underline{\mathcal{I}}_z) \\ & \times \left\langle \frac{\delta g_{\text{ns,LT}}^a}{\pi} \right\rangle_{\text{FS}} (\cot \delta - in_s(0) \underline{\mathcal{I}}_z) \\ & = (X \underline{\mathcal{I}}_x + Y \underline{\mathcal{I}}_y) \langle \alpha_1(\hat{k}_z) \rangle_{\text{FS}} \left(-\frac{\Gamma_{\text{imp}} \gamma \epsilon v_{\text{F}} \Delta_{\text{eq}}(-\partial_y T)}{T^2 \cosh\left(\frac{\epsilon}{2T}\right)} \right). \end{aligned} \quad (\text{B9})$$

From the Eq. (B8), we make an ansatz for the anomalous Keldysh impurity self-energy,

$$\begin{aligned} \delta \underline{\sigma}_{\text{imp,LT}}^a & = \left(\tilde{X} \underline{\mathcal{I}}_x + \tilde{Y} \underline{\mathcal{I}}_y \right) \langle \alpha_1(\hat{k}_z) \rangle_{\text{FS}} \\ & \times \left(-\frac{\Gamma_{\text{imp}} \gamma \epsilon v_{\text{F}} \Delta_{\text{eq}}(-\partial_y T)}{T^2 \cosh\left(\frac{\epsilon}{2T}\right)} \right). \end{aligned} \quad (\text{B10})$$

With this anomalous Keldysh impurity self-energy, we transform the T -matrix equation (B8) into,

$$\begin{pmatrix} 1 - 2\Gamma_{\text{imp}} |\Delta_{\text{eq}}|^2 Y \langle \alpha_2(\hat{k}_z) \rangle_{\text{FS}} & -2\Gamma_{\text{imp}} |\Delta_{\text{eq}}|^2 X \langle \alpha_2(\hat{k}_z) \rangle_{\text{FS}} \\ 2\Gamma_{\text{imp}} |\Delta_{\text{eq}}|^2 X \langle \alpha_2(\hat{k}_z) \rangle_{\text{FS}} & 1 - 2\Gamma_{\text{imp}} |\Delta_{\text{eq}}|^2 Y \langle \alpha_2(\hat{k}_z) \rangle_{\text{FS}} \end{pmatrix} \begin{pmatrix} \tilde{X} \\ \tilde{Y} \end{pmatrix} = \begin{pmatrix} X \\ Y \end{pmatrix}. \quad (\text{B11})$$

From the matrix equation (B11), we obtain the coefficient for the anomalous Keldysh impurity self-energy, \tilde{X} , \tilde{Y} ,

$$\tilde{X} = \frac{X}{\text{Det}}, \quad (\text{B12})$$

$$\tilde{Y} = \frac{Y}{\text{Det}} - \frac{\Gamma_{\text{imp}} |\Delta_{\text{eq}}|^2 \langle \alpha_2(\hat{k}_z) \rangle_{\text{FS}}}{8 \text{Det} (\cot^2 \delta + n_s^2(0))^2}, \quad (\text{B13})$$

where Det represents the determinant of the matrix in Eq. (B11),

$$\begin{aligned} \text{Det} & = 1 - \frac{\Gamma_{\text{imp}} |\Delta_{\text{eq}}|^2 (\cot^2 \delta - n_s^2(0))}{(\cot^2 \delta + n_s^2(0))^2} \langle \alpha_2(\hat{k}_z) \rangle_{\text{FS}} \\ & + \frac{\Gamma_{\text{imp}}^2 |\Delta_{\text{eq}}|^4}{4(\cot^2 \delta + n_s^2(0))^2} \langle \alpha_2(\hat{k}_z) \rangle_{\text{FS}}^2. \end{aligned} \quad (\text{B14})$$

We now obtain the low temperature formula for thermal conductivities,

$$\begin{aligned} \frac{\kappa_{yy}^{\text{ext}}}{N(\epsilon_{\text{F}})v_{\text{F}}^2} & \simeq \frac{\pi^2 T}{6} \gamma^2 \langle \alpha_0(\hat{k}_z) \rangle_{\text{FS}} \\ & + \frac{\pi^2 \Gamma_{\text{imp}} \gamma^2 |\Delta_{\text{eq}}|^2 T}{3} \tilde{Y} \langle \alpha_1(\hat{k}_z) \rangle_{\text{FS}}^2 + \mathcal{O}(T^2), \end{aligned} \quad (\text{B15})$$

$$\frac{\kappa_{xy}^{\text{ext}}}{N(\epsilon_{\text{F}})v_{\text{F}}^2} \simeq -\frac{\pi^2 \Gamma_{\text{imp}} \gamma^2 |\Delta_{\text{eq}}|^2 T}{3} \tilde{X} \langle \alpha_1(\hat{k}_z) \rangle_{\text{FS}}^2 + \mathcal{O}(T^2). \quad (\text{B16})$$

In the clean system $\Gamma_{\text{imp}} \ll \pi T_c$, the low temperature formula for the thermal conductivity reduces to Eqs. (25)

and (26),

$$\begin{aligned} \frac{\kappa_{yy}^{\text{ext}}}{N(\epsilon_{\text{F}})v_{\text{F}}^2} & \simeq \frac{\pi^2 T}{6} \gamma^2 \langle \alpha_0(\hat{k}_z) \rangle_{\text{FS}} \\ & + \frac{\pi^2 \Gamma_{\text{imp}} \gamma^2 |\Delta_{\text{eq}}|^2 T}{3} Y \langle \alpha_1(\hat{k}_z) \rangle_{\text{FS}}^2 \\ & + \mathcal{O}(T^2, \Gamma_{\text{imp}}^4), \end{aligned} \quad (\text{B17})$$

$$\begin{aligned} \frac{\kappa_{xy}^{\text{ext}}}{N(\epsilon_{\text{F}})v_{\text{F}}^2} & \simeq -\frac{\pi^2 \Gamma_{\text{imp}} \gamma^2 |\Delta_{\text{eq}}|^2 T}{3} X \langle \alpha_1(\hat{k}_z) \rangle_{\text{FS}}^2 \\ & + \mathcal{O}(T^2, \Gamma_{\text{imp}}^4). \end{aligned} \quad (\text{B18})$$

Appendix C: Derivation of Eq. (30)

We give the derivation of Eq. (30) to clarify the relation between the extrinsic ATHE and the formation of the impurity band. To associate these, we consider the equilibrium T -matrix equation and the zero-energy DOS. Differentiating Eqs. (B6) and (B7) with the scattering phase-shift, we obtain

$$\frac{\partial \gamma}{\partial(\cot \delta)} = 4 \left(Y \frac{\partial n_s(0)}{\partial(\cot \delta)} - X \right), \quad (\text{C1})$$

$$\frac{\partial n_s(0)}{\partial(\cot \delta)} = |\Delta_{\text{eq}}|^2 \langle \alpha_2(\hat{k}_z) \rangle_{\text{FS}} \frac{\partial \gamma}{\partial(\cot \delta)}, \quad (\text{C2})$$

From Eqs. (C1) and (C2), we obtain

$$\begin{aligned} \frac{\partial n_s(0)}{\partial \delta} \sin^2 \delta & = 4\Gamma_{\text{imp}} |\Delta_{\text{eq}}|^2 \langle \alpha_1(\hat{k}_z) \rangle_{\text{FS}} X \\ & + \mathcal{O}(\Gamma_{\text{imp}}^2). \end{aligned} \quad (\text{C3})$$

Comparing Eq. (26) to Eq. (C3), we find

$$\begin{aligned} \frac{\kappa_{xy}^{\text{ext}}}{N(\epsilon_{\text{F}})v_{\text{F}}^2} & = -\frac{\pi^2 \Gamma_{\text{imp}} \gamma^2 T}{12} \frac{\langle \alpha_1(\hat{k}_z) \rangle_{\text{FS}}^2}{\langle \alpha_2(\hat{k}_z) \rangle_{\text{FS}}} \frac{\partial n_s(0)}{\partial \delta} \sin^2 \delta \\ & + \mathcal{O}(T^2, \Gamma_{\text{imp}}^4). \end{aligned} \quad (\text{C4})$$

-
- [1] G. E. Volovic, *The Universe in a Helium Droplet* (Oxford, 2003).
- [2] D. Xiao, M.-C. Chang, and Q. Niu, *Rev. Mod. Phys.* **82**, 1959 (2010).
- [3] P. Hosur and X. Qi, *Comptes Rendus Physique* **14**, 857 (2013).
- [4] B. Yan and C. Felser, *Ann. Rev. Condens. Matter Phys.* **8**, 337 (2017).
- [5] C. Kallin and J. Berlinsky, *Rep. Prog. Phys.* **79**, 054502 (2016).
- [6] N. Read and D. Green, *Phys. Rev. B* **61**, 10267 (2000).
- [7] H. Sumiyoshi and S. Fujimoto, *J. Phys. Soc. Jpn.* **82**, 023602 (2013).
- [8] A. Balatskii, G. Volovik, and A. Konyshev, *Zh. Eksp. Teor. Fiz* **90**, 2038 (1986).
- [9] T. Matsushita, T. Liu, T. Mizushima, and S. Fujimoto, *Phys. Rev. B* **97**, 134519 (2018).
- [10] T. Kobayashi, T. Matsushita, T. Mizushima, A. Tsuruta, and S. Fujimoto, *Phys. Rev. Lett.* **121**, 207002 (2018).
- [11] Y. Ishihara, T. Mizushima, A. Tsuruta, and S. Fujimoto, *Phys. Rev. B* **99**, 024513 (2019).
- [12] J. Nissinen, *Phys. Rev. Lett.* **124**, 117002 (2020).
- [13] J. Nissinen and G. Volovik, *Phys. Rev. Research* **2**, 033269 (2020).
- [14] T. Meng and L. Balents, *Phys. Rev. B* **86**, 054504 (2012).
- [15] P. Goswami and L. Balicas, arXiv:1312.3632 (2013).
- [16] P. Goswami and A. H. Nevidomskyy, *Phys. Rev. B* **92**, 214504 (2015).
- [17] R. Nakai, S. Ryu, and K. Nomura, *Phys. Rev. B* **95**, 165405 (2017).
- [18] R. Nakai and K. Nomura, *Phys. Rev. B* **101**, 094510 (2020).
- [19] Y. Moriya, T. Matsushita, M. G. Yamada, T. Mizushima, and S. Fujimoto, *J. Phys. Soc. Jpn.* **91**, 094710 (2022).
- [20] B. Arfi, H. Bahlouli, C. J. Pethick, and D. Pines, *Phys. Rev. Lett.* **60**, 2206 (1988).
- [21] S. Li, A. V. Andreev, and B. Z. Spivak, *Phys. Rev. B* **92**, 100506 (2015).
- [22] S. Yip, *Supercond. Sci. Tech.* **29**, 085006 (2016).
- [23] F. Yilmaz and S. Yip, *Phys. Rev. Research* **2**, 023223 (2020).
- [24] V. Ngampruetikorn and J. Sauls, *Phys. Rev. Lett.* **124**, 157002 (2020).
- [25] V. Ngampruetikorn and J. A. Sauls, *Front. Phys.* **12** (2024).
- [26] P. Hirschfeld, P. Wölfle, and D. Einzel, *Phys. Rev. B* **37**, 83 (1988).
- [27] A. V. Balatsky, I. Vekhter, and J.-X. Zhu, *Rev. Mod. Phys.* **78**, 373 (2006).
- [28] T. Matsushita, J. Ando, Y. Masaki, T. Mizushima, S. Fujimoto, and I. Vekhter, *Phys. Rev. Lett.* **128**, 097001 (2022).
- [29] T. Matsushita, T. Mizushima, Y. Masaki, S. Fujimoto, and I. Vekhter, arXiv:2404.02633 (2024).
- [30] A. J. Leggett, *Rev. Mod. Phys.* **47**, 331 (1975).
- [31] M. A. Silaev and G. E. Volovik, *JETP* **119**, 1042 (2014).
- [32] T. Mizushima, Y. Tsutsumi, T. Kawakami, M. Sato, M. Ichioka, and K. Machida, *J. Phys. Soc. Jpn.* **85**, 022001 (2016).
- [33] H. Ikegami, Y. Tsutsumi, and K. Kono, *Science* **341**, 59 (2013).
- [34] H. Ikegami, Y. Tsutsumi, and K. Kono, *J. Phys. Soc. Jpn.* **84**, 044602 (2015).
- [35] O. Shevtsov and J. A. Sauls, *Phys. Rev. B* **94**, 064511 (2016).
- [36] Y. Kasahara, H. Shishido, T. Shibauchi, Y. Haga, T. Matsuda, Y. Onuki, and Y. Matsuda, *New J. Phys.* **11**, 055061 (2009).
- [37] S. Kittaka, Y. Shimizu, T. Sakakibara, Y. Haga, E. Yamamoto, Y. Onuki, Y. Tsutsumi, T. Nomoto, H. Ikeda, and K. Machida, *J. Phys. Soc. Jpn.* **85**, 033704 (2016).
- [38] E. Schemm, R. Baumbach, P. Tobash, F. Ronning, E. Bauer, and A. Kapitulnik, *Phys. Rev. B* **91**, 140506 (2015).
- [39] T. Yamashita, Y. Shimoyama, Y. Haga, T. Matsuda, E. Yamamoto, Y. Onuki, H. Sumiyoshi, S. Fujimoto, A. Levchenko, T. Shibauchi, et al., *Nat. Phys.* **11**, 17 (2015).
- [40] H. Sumiyoshi and S. Fujimoto, *Phys. Rev. B* **90**, 184518 (2014).
- [41] G. Stewart, Z. Fisk, J. Willis, and J. Smith, in *Ten Years of Superconductivity: 1980–1990* (Springer, 1984), pp. 85–88.
- [42] J. Sauls, *Adv. Phys.* **43**, 113 (1994).
- [43] E. Schemm, W. Gannon, C. Wishne, W. Halperin, and A. Kapitulnik, *Science* **345**, 190 (2014).
- [44] K. Izawa, Y. Machida, A. Itoh, Y. So, K. Ota, Y. Haga, E. Yamamoto, N. Kimura, Y. Onuki, Y. Tsutsumi, et al., *J. Phys. Soc. Jpn.* **83**, 061013 (2014).
- [45] Y. Tsutsumi, M. Ishikawa, T. Kawakami, T. Mizushima, M. Sato, M. Ichioka, and K. Machida, *J. Phys. Soc. Jpn.* **82**, 113707 (2013).
- [46] Y. Tsutsumi, K. Machida, T. Ohmi, and M.-a. Ozaki, *J. Phys. Soc. Jpn.* **81**, 074717 (2012).
- [47] Y. Yanase, *Phys. Rev. B* **94**, 174502 (2016).
- [48] H. Ott, H. Rudigier, Z. Fisk, and J. Smith, *Phys. Rev. Lett.* **50**, 1595 (1983).
- [49] Y. Shimizu, S. Kittaka, S. Nakamura, T. Sakakibara, D. Aoki, Y. Homma, A. Nakamura, and K. Machida, *Phys. Rev. B* **96**, 100505 (2017).
- [50] B. Golding, D. Bishop, B. Batlogg, W. Haemmerle, Z. Fisk, J. Smith, and H. Ott, *Physical Rev. Lett.* **55**, 2479 (1985).
- [51] B. Batlogg, D. Bishop, B. Golding, C. M. Varma, Z. Fisk, J. L. Smith, and H. R. Ott, *Phys. Rev. Lett.* **55**, 1319 (1985).
- [52] T. Mizushima and M. Nitta, *Phys. Rev. B* **97**, 024506 (2018).
- [53] K. Machida, *J. Phys. Soc. Jpn.* **87**, 033703 (2018).
- [54] P. K. Biswas, H. Luetkens, T. Neupert, T. Stürzer, C. Baines, G. Pascua, A. P. Schnyder, M. H. Fischer, J. Goryo, M. R. Lees, et al., *Phys. Rev. B* **87**, 180503 (2013).
- [55] M. H. Fischer, T. Neupert, C. Platt, A. P. Schnyder, W. Hanke, J. Goryo, R. Thomale, and M. Sgrist, *Phys. Rev. B* **89**, 020509 (2014).
- [56] S. Adenwalla, S. Lin, Q. Ran, Z. Zhao, J. B. Ketterson, J. A. Sauls, L. Taillefer, D. Hinks, M. Levy, and B. K. Sarma, *Phys. Rev. Lett.* **65**, 2298 (1990).
- [57] K. Hasselbach, L. Taillefer, and J. Flouquet, *Phys. Rev. Lett.* **63**, 93 (1989).

- [58] H. Ott, H. Rudigier, Z. Fisk, and J. Smith, *Phys. Rev. B* **31**, 1651 (1985).
- [59] J. Kim, B. Andraka, and G. Stewart, *Phys. Rev. B* **44**, 6921 (1991).
- [60] U. Rauchschwalbe, C. Bredi, F. Steglich, K. Maki, and P. Fulde, *Europhys. Lett.* **3**, 757 (1987).
- [61] R. H. Heffner, J. L. Smith, J. O. Willis, P. Birrer, C. Baines, F. N. Gygax, B. Hitti, E. Lippelt, H. R. Ott, A. Schenck, et al., *Phys. Rev. Lett.* **65**, 2816 (1990).
- [62] K. Machida and T. Ohmi, *Phys. Rev. Lett.* **86**, 850 (2001).
- [63] V. P. Mineev, *Phys. Rev. B* **66**, 134504 (2002).
- [64] V. P. Mineev, *Phys. Rev. B* **90**, 064506 (2014).
- [65] J. D. Sau and S. Tewari, *Phys. Rev. B* **86**, 104509 (2012).
- [66] N. T. Huy, A. Gasparini, D. E. de Nijs, Y. Huang, J. C. P. Klaasse, T. Gortenmulder, A. de Visser, A. Hamann, T. Görlach, and H. v. Löhneysen, *Phys. Rev. Lett.* **99**, 067006 (2007).
- [67] V. Mineev, *Phys. Rev. B* **95**, 104501 (2017).
- [68] D. Aoki, A. Huxley, E. Ressouche, D. Braithwaite, J. Flouquet, J.-P. Brison, E. Lhotel, and C. Paulsen, *Nature* **413**, 613 (2001).
- [69] S. Saxena, P. Agarwal, K. Ahilan, F. Grosche, R. Haselwimmer, M. Steiner, E. Pugh, I. Walker, S. Julian, P. Monthoux, et al., *Nature* **406**, 587 (2000).
- [70] Y. Tanaka, M. Sato, and N. Nagaosa, *Journal of the Physical Society of Japan* **81**, 011013 (2011).
- [71] M. Sato and S. Fujimoto, *J. Phys. Soc. Jpn* **85**, 072001 (2016).
- [72] M. Sato and Y. Ando, *Rep. Prog. Phys.* **80**, 076501 (2017).
- [73] K. Nomura, S. Ryu, A. Furusaki, and N. Nagaosa, *Phys. Rev. Lett.* **108**, 026802 (2012).
- [74] T. Qin, Q. Niu, and J. Shi, *Phys. Rev. Lett.* **107**, 236601 (2011).
- [75] A. Shitade, *Prog. Theor. Expe. Phys.* **2014** (2014).
- [76] M. Sigrist and K. Ueda, *Rev. Mod. Phys.* **63**, 239 (1991).
- [77] G. Eilenberger, *Z. Physik* **214**, 195 (1968).
- [78] J. Serene and D. Rainer, *Phys. Rep.* **101**, 221 (1983).
- [79] M. Stone, *Phys. Rev. B* **85**, 184503 (2012).
- [80] M. J. Graf, S.-K. Yip, J. A. Sauls, and D. Rainer, *Phys. Rev. B* **53**, 15147 (1996).
- [81] A. B. Vorontsov and I. Vekhter, *Phys. Rev. B* **75**, 224502 (2007).
- [82] N. Nagaosa, J. Sinova, S. Onoda, A. H. MacDonald, and N. P. Ong, *Rev. Mod. Phys.* **82**, 1539 (2010).
- [83] N. Sinitsyn, A. MacDonald, T. Jungwirth, V. Dugaev, and J. Sinova, *Phys. Rev. B* **75**, 045315 (2007).
- [84] See the appendix for the detail calculations.
- [85] Y. Maeno, S. Yonezawa, and A. Ramires, *arXiv:2402.12117* (2024).